Macromolecules

pubs.acs.org/Macromolecules
Article

Dynamics of End-Functionalized Weakly Entangled Polyethylene-Oxide in the Melt

Margarita Kruteva,* Jürgen Allgaier, Barbara Gold, Wim Pyckhout-Hintzen, Andreas Raba, Aurel Radulescu, Andreas Wischnewski, Michael Monkenbusch, Peter Falus, and Dieter Richter

Cite This: Macromolecules 2026, 59, 3508−3517

ABSTRACT: Extending an earlier study on short unentangled telechelic poly(ethylene oxide) (PEO2K) chains by Monkenbusch et al. (*Phys Rev Lett* **2016**, *117* (14), 147802), we present investigations on the association dynamics of weakly entangled PEO8K using pulsed field gradient nuclear magnetic resonance (PFG-NMR), small angle neutron scattering (SANS) and neutron spin echo (NSE). From PFG-NMR we obtain the average Fickian diffusion coefficients. With increasing temperature, they approach those from the neat unfunctionalized melt indicating diminishing aggregation. A random phase approximation (RPA) evaluation of SANS data results in much weaker aggregation compared to the PEO2K counterpart in agreement with the prediction of Caruthers' law. The picture of mode amplitude suppression as proposed by Monkenbusch et al. is supported. As a consequence of the rather long terminal times of PEO8K compared to the bond lifetimes, the NSE spectra from the functionalized melt may be well approximated by a product of the internal relaxation spectrum of the building block and the modified diffusion dynamics of the aggregates. Finally, the average center of mass diffusion of the ensemble of aggregates is quantitatively described in terms of the structural SANS results and the aggregation statistics extrapolated from earlier work.

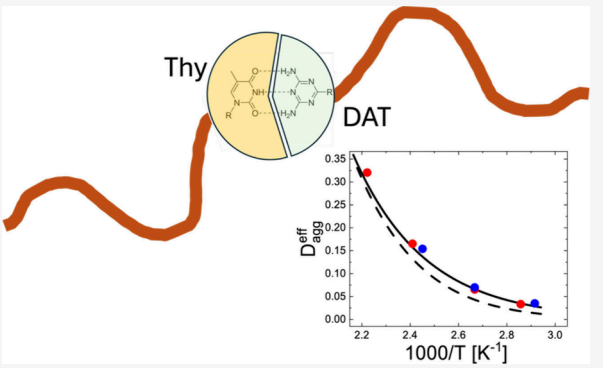

INTRODUCTION

Presently, supramolecular polymer systems with transient polymer interactions are much investigated.[1−16] Polymers functionalized with reversible linkers form an emerging class of polymers that offer superior properties compared to their nonassociating counterparts. Such polymers demonstrate novel properties such as sensors, self-healing, responsiveness, or shape memory materials. Depending on temperature or pH value, such functionalized polymers may behave like permanent networks or even though the building blocks may be small, exhibit high viscosities like high M_W materials. The transient interactions are commonly enabled by hydrogen bonding, metal complexation, ionic forces or π-π stacking. H-bonds are directional allowing selective strength by self- and heterocomplementarity. Their strength may be tuned, e.g., by the number of acting bonds, their geometry, etc. Also, they play an important role in biocompatibility, e.g., in tissue engineering.[17]

The properties relate to thermodynamic equilibrium structure and very importantly on the dynamics of the associates and the interplay between hydrogen bonding and chain dynamics. The H-bonding dynamics previously was studied in solution or for very low molecular weights. Sokolov et al. studied H-bonding interactions in telechelic poly(propylene glycol) (PPG) and polydimethylsiloxane (PDMS) by dielectric methods together with rheology.[1] They observed a slowdown of segmental dynamics together with an increase of the glass transition temperature T_g. The different properties of these materials were explained by the significantly different relation between bond- and chain dynamics. Also partner exchange rates are important for viscoelastic effects. Associative polymer dynamics also characterizes vitrimers representing novel materials with properties such as self-healing or easy recyclability.[2]

Employing a Poisson renewal model, early treatments of the stress relaxation in entangled supramolecular polymers were reported by Granek and Cates.[3] More detailed theoretical approaches were undertaken, e.g., by Stukalin and Freed.[18] Again, based on the Poisson renewal approach for Rouse chains they derived explicit results for the complex viscosity and the dielectric response from the chain end-to-end vector. If bond-breaking rates are in the order of the structural chain relaxation times, both theories predict that the interplay

Received: December 25, 2025
Revised: February 7, 2026
Accepted: February 18, 2026
Published: March 3, 2026

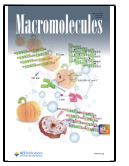

https://doi.org/10.1021/acs.macromol.5c03604
Macromolecules 2026, 59, 3508−3517

between scission dynamics and structural relaxation accelerates the stress relaxation. Leibler et al. and Rubinstein and Semenov proposed a sticky Rouse or reptation model to explain structure, dynamics and viscoelastic response of supramolecular polymers.[5,6]

Recently we studied associating telechelic polymers (PEO) with heterocompatible diaminotriazine and Thymine (DAT and Thy) functional groups at the ends (triple H-bonds) by small angle scattering (SAXS and SANS).[7] Using different labeling schemes SANS showed exclusively linear aggregation. Pulsed field gradient nuclear magnetic resonance (PFG-NMR) and viscosity measurements displayed prevailing Rouse dynamics. The chain length distribution was compatible with polycondensation statistics. The observation of Rouse type relaxation even for larger aggregates indicated that the bond lifetimes were too short to establish an entanglement network. However, a quantitative evaluation of the bond lifetime remained elusive.

Very recently we investigated the dynamics of such telechelic polymers on a microscopic scale enabling a direct microscopic determination of the bond relaxation time τ_b and elucidating the microscopic mechanism of the interplay between chain and dissociation dynamics.[19] In disagreement to former theoretical explanations, we found that the interplay between chain and bond dynamics results in a reduction of the mode amplitudes of long wavelength Rouse modes rather than in a modification of the mode relaxation rates by adding bond breaking and mode relaxation rates. For modes with longer relaxation times than the bond lifetime the entropic restoring force is interrupted upon chain cleavage; the affected modes do not further contribute to the relaxation process. Thus, the effective rate is reduced and not accelerated as former approaches predicted.

Employing pulsed field gradient nuclear magnetic resonance (PFG-NMR), SANS and neutron spin echo (NSE), in this work we extend the earlier approach of Monkenbusch et al., where the supramolecular building blocks were short Rouse chains, to weakly entangled PEO-polymers encompassing about 4 entanglements. (i) PFG-NMR delivers diffusion coefficients that with increasing temperature are approaching those from the neat melt indicating diminishing aggregation. (ii) RPA evaluation of SANS data results in much weaker aggregation compared to the PEO2K counterpart in agreement with the prediction of Caruthers' law (iii) The picture of loss of mode contributions instead of addition of chain and bond relaxation rates as presented by Monkenbusch et al. is supported. (iv) As a consequence of the rather long terminal times of PEO with a molecular weight 8 kg/mol (PEO8K) compared to the bond lifetimes, the NSE-spectra from the functionalized melt may be understood as a product of the internal relaxation spectrum of the building block and the modified diffusion dynamics of the aggregates. (v) Finally, the average center of mass diffusion of the ensemble of aggregates is quantitatively described in terms of the structural results from SANS and the aggregation statistics extrapolated from earlier work.

MODIFIED ROUSE THEORY WITH MODE SUPPRESSION AND MODE LIFETIME

In a recent work by Monkenbusch et al. the dynamics of associating functionalized polymers for the case of short unentangled PEO chains with a molecular weight of 2 kg/mol (PEO2K) was investigated. As the main insight the authors realized that the finite lifetime of the hydrogen bonded links did not affect the mode relaxation times but the weight of mode contribution (technically implemented by reduction of the mode amplitudes). Rouse modes of an aggregate are no longer contributing to the chain relaxation, if the entropic pull ceases after breaking of the aggregate. This observation was implemented into the Rouse dynamic structure factor by a factor $\exp\left[-\frac{\tau_p}{\tau_{agg}}\right]$ modifying the amplitude of a mode with relaxation time τ_p.

In this work we deal with associating end functionalized PEO chains, where the building blocks are weakly entangled, with a molecular weight of 8 kg/mol (PEO8K). The number of entanglements per chain was equal to $Z = 4$. Sharma et al. have shown that the effect of topological constraints in weakly entangled melts may be well described by the suppression of Rouse relaxation modes with a length scale larger than the entanglement distance N_e or tube diameter d.[20] With this the dynamic structure factor for a melt of supramolecular weakly entangled polymers becomes

$$S(Q,t) = \sum_{N_{agg}=1}^{\infty} W_{chain}(N_{agg}) \left(\sum_{n=h}^{h+N_{agg}} \sum_{m=h}^{h+N_{agg}} \exp[-Q^2 \phi_{n,m}^{N_0 N_{agg}}(t)] \right) \tag{1}$$

with

$$\begin{aligned} \phi_{n,m}^{N_0 N_{agg}}(t) = {} & D_{com}^{N_{agg}} t + \frac{|n-m|}{6} l_{seg}^{\,2} + \frac{2 N_{agg} N_0 l_{seg}^{\,2}}{3\pi^2} \\ & \times \sum_{p=1}^{N_0 N_{agg}} \frac{1}{p^2} f(p) \left(1 - \exp\left[-\frac{t}{\tau_p}\right]\right) \\ & \times \cos\left(\frac{\pi p n}{N}\right) \cos\left(\frac{\pi p m}{N}\right) \exp\left[-\frac{\tau_p}{\tau_{agg}}\right] \end{aligned} \tag{2}$$

where $W_{chain}(N)$ is the chain length distribution, N_0 is the monomer number of the functionalized polymer building block, l_{seg} is the monomer length, N_{agg} is the aggregation number, $D_{com}^{N_{agg}}$ is the diffusion coefficient for aggregate with N_{agg} components, p is the Rouse mode number, τ_p is the relaxation time of mode p, and τ_{agg} is a lifetime of aggregate. Mode suppression is described by a Fermi-function $f(p) = \left(1 + \exp\left[\frac{p_{cross} - p}{p_{width}}\right]\right)^{-1}$; p_{cross} is the mode number of the transition center of mode suppression and p_{width} describes its extension. For the translational diffusion we assumed subdiffusive behavior at short times crossing over to Fickian diffusion at longer times. The random labeling situation is considered by restricting the sums over the beads n, m to the region of one single selected labeled building block starting at bead h. The time dependent center of mass mean squared displacement (MSD) was modeled as

$$\begin{aligned} & \langle r_{com}^{\,2}(t) \rangle \\ & = \left(\left(\exp[-\ln(\langle r_0^{\,2} \rangle / 6 D_{Fick}) \mu] \langle r_0^{\,2} \rangle t^{\mu} \right)^{a_{cross}} + (6 D_{Fick} t)^{a_{cross}} \right)^{1/a_{cross}} \end{aligned} \tag{3}$$

where D_{Fick} is the long time Fickian diffusion coefficient, μ is the exponent for subdiffusion, $\langle r_0^{\,2} \rangle$ the center of mass MSD at the cross over from sub- to Fickian diffusion, and a_{cross} describes the sharpness of the cross over. We took $a_{cross} = 8$.

https://doi.org/10.1021/acs.macromol.5c03604
Macromolecules 2026, 59, 3508−3517

EXPERIMENT

Synthesis and Sample Preparation

Synthesis and characterization are described in the Supporting Information. The chemical structure of the end groups functionalizing the PEO chains and their configuration in hydrogen bonding are displayed in Figure 1:

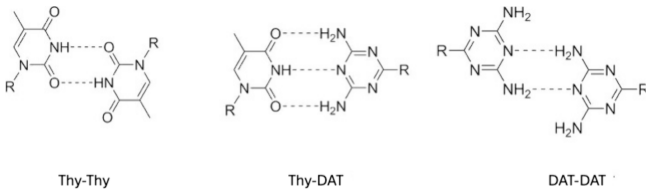

Figure 1. Chemical structure of the functionalizing end-groups thy and DAT and their configuration in hydrogen bonding. Binding equal end-groups two hydrogen bonds are active, while for hetero bonding 3 hydrogen bonds are involved.

For a characterization by DSC see refs 21 and 22.

Two differently labeled supramolecular melts were prepared by solution blending and subsequent drying under high vacuum conditions. The sample for SANS contained 50% of hydrogenated and 50% deuterated polymer heterocompatible Thy-PEO8K-Thy and DAT- PEO8K-DAT. In this way by association an alternating h-d copolymer is created. To avoid cross-terms between different "h" and "d" components the NSE sample contained equal amounts (volume fraction ϕ_{1-4} = 0.25) of all four well monodisperse (Table 1) building blocks:

Table 1. Characteristics of the Functionalized PEO Samples[a]

Material	M_w [kg/mol]	M_n [kg/mol]	M_w/M_n	N
Thy-hPEO8K-Thy	8201	8120	1.01	185
Thy-dPEO8K-Thy	8858	8770	1.01	183
DAT-hPEO8K-DAT	8090	8010	1.01	182
DAT-dPEO8K-DAT	8767	8680	1.01	180

[a]Weight averaged molecular weight, M_w; number averaged molecular weight, M_n; molecular weight distribution, M_w/M_n; number of segments per polymer chain, N.

Thy-hPEO8K-Thy, Thy-dPEO8K-Thy, DAT-hPEO8K-DAT, and DAT-dPEO8K-DAT. This leads to a random scattering contrast that results in a zero average of all interferences between scattering contributions from different blocks.

Pulsed Field Gradient NMR (PFG-NMR)

The PFG-NMR measurements were performed using a magnetic resonance analyzer Bruker Minispec (mq20) operating at ^{1}H frequency of 20 MHz and equipped with a permanent magnet. The attenuation of the echo signal from a pulse sequence containing a magnetic field gradient pulse is used to measure the translational diffusion of the molecules (protons) in the sample at the time scale of tens of milliseconds. During this time the protons overcome the distances of order of hundreds of nanometres, much larger than the size of the chains or their aggregates. Thus, PFG-NMR measures the center-of-mass diffusion. Diffusion coefficient was measured using a standard stimulated echo pulsed-field-gradient (STE) sequence[23] in the temperature interval from 333 to 413 K.

The diffusion attenuation curve is determined by the equation

$$A(g^2)/A(0) = \exp(-q^2(\Delta - \delta/3)D) \quad (4)$$

where $q = g\gamma\delta$ is a generalized momentum transfer or scattering vector[24] with g and δ being the magnetic field gradient strength and duration respectively and γ is the proton gyromagnetic ratio. Δ is the diffusion time and D is the diffusion coefficient.[23]

Small Angle Neutron Scattering (SANS)

The SANS experiments were carried out at the KWS-2 instrument at the MLZ (Munich, Germany).[25] The absolute scattering intensities were measured over a scattering vector range of $0.008 < Q < 0.5$ Å^{-1} using neutrons with $\lambda = 5$ Å and sample-to-detector distances between 1 and 8 m with corresponding collimation lengths. The conversion to absolute scale intensities was performed using a 1.5 mm thick Plexiglas plate, which served as a secondary standard sample. The experimental two-dimensional data were corrected in a standard fashion for background and empty cell scattering as well as detector sensitivity before being radially averaged. Since the melting point of poly(ethylene oxide) is around 323 K, the measurement temperatures were 343, 375, and 408 K.

Neutron Spin Echo (NSE)

The neutron spin echo experiments were performed at the Institute Laue Langevin in Grenoble. At neutron wavelengths of 10 and 13.5 Å covering a time range from 0.1 to 500 ns. The accessed momentum transfers were Q = 0.05, 0.077, 0.096, 0.13, 0.15 Å^{-1}. As a reference a neat PEO8K melt was investigated.[26] The background was obtained from a fully deuterated PEO8K sample and subtracted. Four different temperatures were investigated: 350, 375, 415, and 450 K.

RESULTS

The Thy and DAT end-functionalized PEOs were synthesized using a method, first described for the functionalization of poly(1,2-butylene oxide).[27] In addition, DAT functionalization was improved by replacing the low molecular weight DAT functionalization agent 2-chloro-4,6-diamino-1,3,5-triazine by its more reactive fluoro-analogue 2-fluoro-4,6-diamino-1,3,5-triazine. The details are described in the Supporting Information. The functionalization degrees of the supramolecularly functionalized PEOs were determined using ^{1}H NMR by comparing the signal intensities of the PEO signals with the end group signal intensities. The PEO signal intensities were calibrated from measurements of the starting polymers tBu-O-hPEO8k-OH and tBu-O-dPEO8k-OH, which contain 9 hydrogen atoms in the tBu starter group at one chain end. For the hydrogenous polymers Thy-hPEO8k-Thy and DAT-hPEO8k-DAT the functionalization degrees of the end groups were 93% and 91%, respectively. The deuterated counterparts Thy-dPEO8k-Thy and DAT-dPEO8k-DAT showed visibly lower functionalization degrees of only 75% and 76%, respectively. Possibly, impurities in the deuterated monomer caused the lower functionalization of the deuterated polymers. Other reasons could not be found as the syntheses were carried out under the same conditions using the identical reagents.

The translational (Fickian) diffusion coefficients both for neat as well as for functionalized PEO8K has been studied by PFG-NMR. The samples used for PFG-NMR experiment were identical to those studied by neutron scattering. The results are

https://doi.org/10.1021/acs.macromol.5c03604
Macromolecules 2026, 59, 3508−3517

presented in Table 2. We note that the melting temperature of PEO has been reported to be in the range 331−340 K.[28]

Table 2. Fickian Diffusion Coefficients Determined by PFG-NMR:[a] (a) Diffusion Coefficients Obtained from Fitting an Arrhenius Law for the Temperatures of the NSE Experiments; (b) Diffusion Coefficients as Measured

(a) Arrhenius Law		
T [K]	D_{PEO8K} [Å^2/ns]	D_{agg} [Å^2/ns]
350	0.079 ± 0.010	0.0348 ± 0.0059
375	0.132 ± 0.012	0.0662 ± 0.0053
415	0.264 ± 0.018	0.157 ± 0.013
450	0.436 ± 0.021	0.296 ± 0.018
(b) As Measured		
T [K]	D_{PEO8K} [Å^2/ns]	D_{agg} [Å^2/ns]
338	0.0490 ± 0.0062	0.0136 ± 0.0012
343	0.0679 ± 0.001	0.0221 ± 0.0020
350	0.098 ± 0.005	0.0373 ± 0.0040
375	0.12 ± 0.001	0.061 ± 0.001
400	0.224 ± 0.007	0.130 ± 0.001
415	0.264 ± 0.003	0.166 ± 0.002
430	0.342 ± 0.006	0.215 ± 0.002
450	0.4210 ± 0.0096	0.280 ± 0.004

[a] D_{PEO8K} for Reference Melt; D_{agg} for Functionalized PEO8K Melt.

Figure 2 displays the PFG-NMR results in an Arrhenius representation.

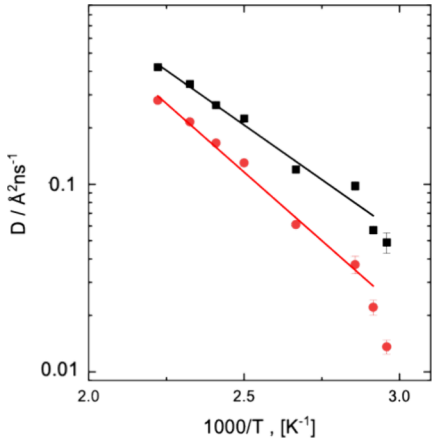

Figure 2. Translational diffusion coefficients measured by PFG-NMR for neat (black symbols) and end-functionalized PEO8K (red symbols) as a function of inverse temperature.

For the neat PEO8K the translational center of mass (com) diffusion was well studied on the NSE scale. There, a pronounced subdiffusive component was found, which for all temperatures could be well described over the full dynamic range by a crossover to Fickian diffusion at an MSD $\langle r_{com}^2(t_{cross})\rangle$ = 1782 ± 16 Å^2 (eq 3). The corresponding subdiffusive exponent was found as μ = 0.529 ± 0.001.

Chain Association Investigated by SANS

In our previous work we studied the structure of a PEO-based supramolecular melt, where chains of 2 kg/mol (PEO2K) (below the entanglement molecular weight) were functionalized each with triple H-bonding Thy and DAT groups at the chain ends.[7] Using isotope labeling for both differently functionalized chains the case of an alternating multiblock copolymer as well as randomly labeled associated blocks were realized. Unlike for most other H-bonding groups and interesting polymers that phase-separate, neat and functionalized PEO share very comparable polarities and homogeneous mixtures result. Therefore, the PEO-Thy-DAT system is nearly ideally suited to study fundamental questions of the correlation between structural and dynamical properties introduced by the supramolecular linking. Whereas Kruteva et al. used unentangled short chains PEO2K,[7] the present work deals with weakly entangled chains bearing on average Z = 4 entanglements. Decades ago, Read[29] presented a useful approach to the random phase approximation that can be applied for the linear association of monodisperse telechelically modified prechains that are arranged in an alternating fashion with the general structure $(AB)_nA$. We refer to the earlier publication for a more detailed discussion of the random-phase-approximation.

The scattering contributions of the A and/or B blocks in such an alternating multiblock copolymer contain intrablock self-terms as well as correlated AA and AB interblock terms, which are separated by a number of blocks. Correlations quickly drop off with distance and the correlation peak in the RPA depends only on the lower association states. In polycondensation theory the association distribution is very broad and non-negligible in the investigated temperature range. Furthermore, as in the former study on short PEO chains, some imperfections may be present. We calculate the RPA-structure factor for the pure multiblock alternating block copolymer as

$$\frac{\frac{d\Sigma}{d\Omega}}{\Delta\rho^2} = S_{RPA} = \frac{S^0_{AA}S^0_{BB} - (S^0_{AB})^2}{S^0_{AA} + S^0_{BB} + 2S^0_{AB}} \tag{5}$$

where $\frac{d\Sigma}{d\Omega}$ is the macroscopic differential cross section and the contrast factor $\Delta\rho^2$. $S^0_{i,j}$ stands for the partial structure factors of each building block:

$$S^0_{AA(BB)}(Q) = \phi_{A(B)}N_{A(B)}\upsilon P_{AA(BB)}(Q) \tag{6}$$

and

$$S^0_{AB}(Q) = \sqrt{N_A N_B \phi_A \phi_B}\,\upsilon P_{AB}(Q) \tag{7}$$

with υ being the monomeric volume, $P_{AA(BB)}$ and P_{AB} consisting both of the involved intra- and interblock terms as defined in the earlier reference by Read[29] and Kruteva et al.;[7] N_A and N_B denote the corresponding chain lengths and ϕ_A and ϕ_B the respective volume fractions in the multiblock copolymer.

As suggested by the sample characterization, we introduce unassociated species. Then the RPA structure factor contributions finally become

$$S^{0,eff}_{AA(BB)}(Q) = \eta\phi_{A(B)}N_{A(B)}\upsilon P_{AA(BB)}(Q) + (1-\eta)S^0_{lin=AA(BB)}(Q) \tag{8}$$

$$S^{0,eff}_{AB}(Q) = \eta S^0_{AB}(Q) \tag{9}$$

The presence of a labeled background from unassociated linear chain species, described by $S^0_{lin=AA(BB)}(Q)$ with a weighting of $(1-\eta)$ is thereby taken into account. As the unassociated species are not spatially correlated, the cross

https://doi.org/10.1021/acs.macromol.5c03604
Macromolecules 2026, 59, 3508−3517

terms are zero and the RPA formulation becomes a weighted mixture of multiblock copolymer and H/D symmetric 50/50 linear chain blend scattering. The latter scattering filling up the correlation hole of the ideal $(AB)_nA$ structure factor. Figure 3 displays this effect for several η, varying between 0 and 100% if the effective correlation functions are used in eq 5.

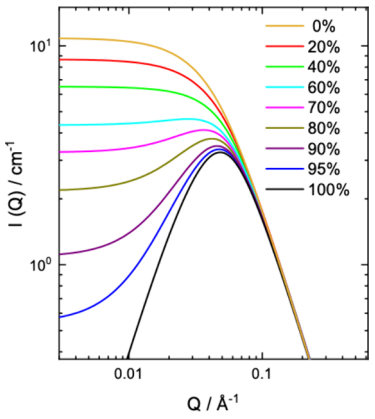

Figure 3. Effect of functionalized PEO chains on the SANS scattering pattern. The legend represents the ratio of the functionalized chains η in the melt.

The generic $(AB)_nA$ supramolecular multiblock copolymer has an association degree "n" of diblock units. Then the total supramolecular association degree is about $2n$ for identical lengths of A and B and $n \rightarrow \infty$. In the following, for shorter aggregates, we will use the aggregation number $(2n - 1)$ being the total number of connected macromonomers. It is estimated from the weight-averaged calculated polymerization degrees $\langle N_{agg} \rangle_w$ in polycondensation theory (see further and eq 11) and fix n in the fitting procedure.

In Figure 4 the SANS data, already corrected for incoherent background and for Porod power-law scattering at the lowest Q ($\sim Q^{-\alpha}$ with exponent $\alpha = 3$ to 4) is shown. We note that the Porod scattering does not interfere in the scattering vector range of interest. The level of the incoherent background was

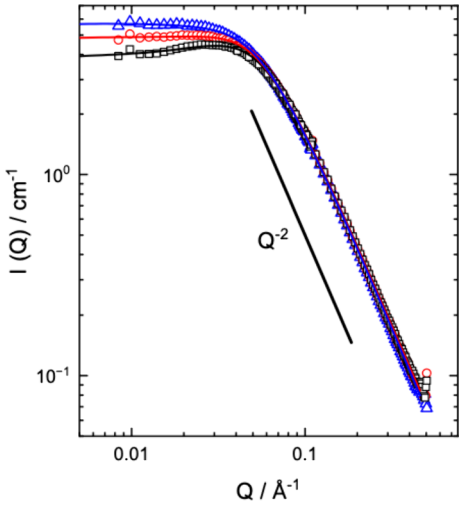

Figure 4. SANS data measured for the functionalized PEO sample at different temperatures: 343 K (black squares), 375 K (red circles) and 408 K (blue triangles) corrected for incoherent background and Porod power-law scattering. The lines are the fits with the eqs 7 and 8.

fitted to 0.38 cm^{-1} and was nearly constant as a function of temperature. The Porod scattering due to voids in the 50% deuterium containing samples was fitted as well and subtracted point-by-point from the data. In view of Figure 3 the absence of an expected pronounced RPA peak is already a strong indication for an enhanced contribution of imperfections or of competing supramolecular reactions. The solid lines represent fits to the 50/50% mixture of functionalized hPEO8K and dPEO8K. In the fitting procedure the number of monomers per strand was fixed; i.e., the average of both components and the contrast factor was kept at the theoretically computed value. The statistical segment length of the effective monomer was refined as (6.2 ± 0.1 Å) on average and absorbs the detailed differences in the individual oligomer chain lengths as well as the number of extra virtual monomers. The fraction of unassociated chains is given by $(1 - \eta)$ and contains both, the statistically unaggregated as well as those unaggregated due to defects. In Table 3 we present both fractions, the difference of

Table 3. Fractions of Aggregated η and Unaggregated $(1 - \eta)$ Chains, Ratio of Statistically Unaggregated Chains, and Net Defects α

T [K]	aggregated fraction η	unaggregated fraction $(1 - \eta)$	statistically unaggregated	net defects α
343	0.64 ± 0.01	0.36	0.04	0.32
375	0.56 ± 0.01	0.44	0.106	0.33
408	0.48 ± 0.01	0.52	0.22	0.3

which denotes the volume fraction of defects. As may be seen, the net defects do not vary with temperature as they should. Furthermore, its magnitude correlates well with the results from the sample characterization.

Chain Dynamics Investigated by NSE

Figure 5 displays the obtained spectra from the sample with random scattering contrast for 4 different temperatures. The NSE Q-range coincides mostly with the asymptotic Q^{-2} behavior of the SANS spectra.

For the lowest (350 K) and the highest (450 K) temperatures Figure 6 compares the spectra from the functionalized polymer melt with those from the reference PEO8K melt.[26] While at 350 K the spectra differ significantly, at 450 K the difference between the spectra is marginal showing that at 450 K we deal with only weakly aggregated chains. On the other hand, the significantly different spectra at 350 K indicate substantial aggregation.

DISCUSSION

Association Properties of the Functionalized PEO8K Chains

We start with describing prior knowledge from the Monkenbusch PEO experiment on short unentangled PEO2K strands carrying Thy or DAT functionalization on both ends[19] and the corresponding SANS study on the same system.[7] There, for the association constant of Thy-DAT we found

$$K_{agg} = 1.46 \times 10^{-4} \exp[4559/T] \quad (10)$$

According to Caruthers[30] the aggregation number follows:

$$N_{agg} = 2K_{agg}[H_0]/((1 + 4K_{agg}[H_0])^{1/2} - 1) \quad (11)$$

https://doi.org/10.1021/acs.macromol.5c03604
Macromolecules 2026, 59, 3508−3517

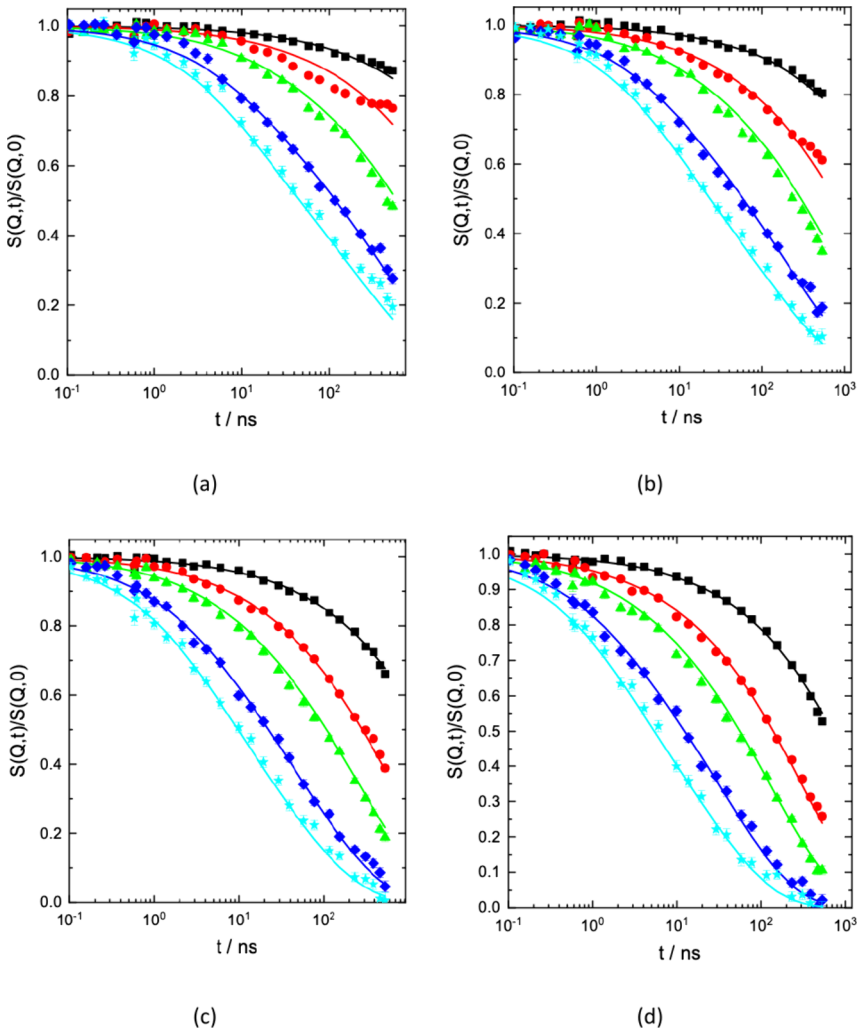

Figure 5. NSE spectra from the sample with random scattering contrast at temperatures 350 K (a), 375 K (b), 415 K(c) and 450 K (d) for Q-values from above: 0.05, 0.077, 0.096, 0.13, 0.15 [Å^{-1}]. For the lines see text.

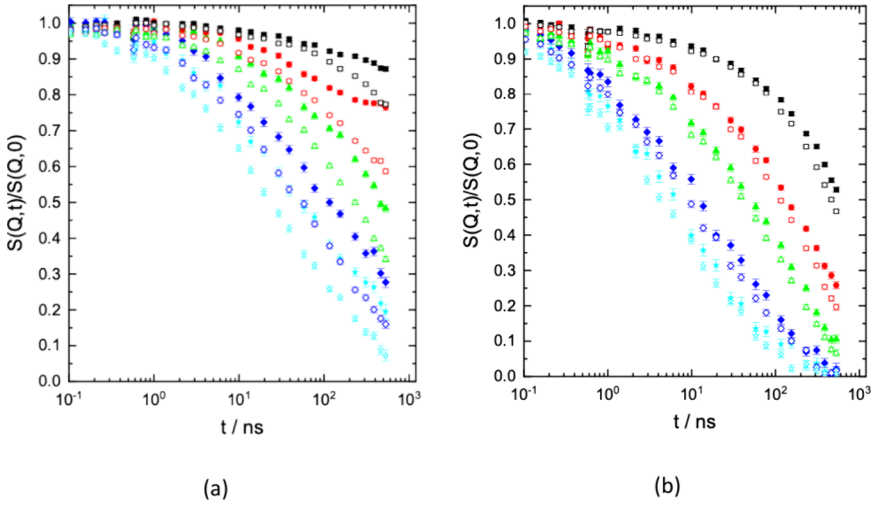

Figure 6. Comparison of the spectra from the corresponding melts of neat PEO8K and functionalized PEO at 350 K (a) and 450 K (b). The empty symbols mark the data from the neat melt; the filled ones display the spectra from the functionalized melt. the spectra differ significantly, at 450 K the difference between the spectra is marginal showing that at 450 K we deal with only weakly aggregated chains. On the other hand, the significantly different spectra at 350 K indicate substantial aggregation.

where $[H_0]$ is the concentration of active groups (hydrogen bonding groups) in mol/L. The distribution of aggregation states according to polycondensation theory follows the Flory distribution:

https://doi.org/10.1021/acs.macromol.5c03604
Macromolecules 2026, 59, 3508−3517

Table 4. Expected Average Aggregation Numbers N_{agg}, Association Probabilities "p" Based on Ref 8[a]

T [K]	N_{agg}	p	$w(1)$	$w(2)$	$w(3)$	$w(4)$	$w(5)$	$w(6)$
350	4.42	0.775	0.0506	0.0784	0.0912	0.09	0.0942	0.0913
375	3.07	0.674	0.106	0.143	0.144	0.130	0.110	0.0888
415	1.99	0.497	0.253	0.251	0.187	0.124	0.0772	0.0460
450	1.54	0.355	0.416	0.295	0.157	0.0744	0.0330	0.0140

[a] $w(i)$ are the aggregate fractions containing "i" building blocks.

$$w(i) = ip^{i-1}(1-p)^2 \tag{12}$$

For the normalized mass distribution of the different aggregates follows

$$mw(i) = i^2 p^{i-1}(1-p)^3/(1+p) \tag{13}$$

With M_0, the mass of the building block, the distribution leads to the number-average mass

$$\langle M_{agg}\rangle_n = \frac{1}{1-p}M_0 \tag{14}$$

and the weight-average mass

$$\langle M_{agg}\rangle_w = \frac{1+p}{1-p}M_0 \tag{15}$$

"p" is the association probability that may be obtained from eqs 11−13. Using K_{agg} and $[H_0]$ = 0.23 mol/L, we obtain the statistical quantities as displayed in Table 4.

Figure 7 displays the corresponding distribution functions for the 4 different temperatures.

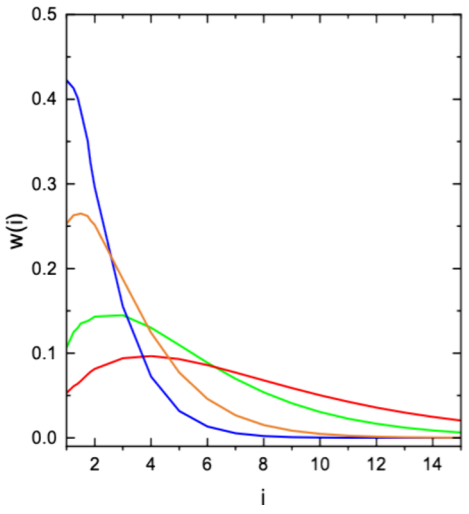

Figure 7. Normalized number distribution of aggregates built by PEO8K chains with Thy-DAT end functionalization: blue, 450 K; orange, 415 K; green, 375 K; red, 350 K.

As may be seen toward lower temperatures the distribution gets very broad and very large aggregates are possible (i = 15 relates to PEO with M_n = 120 kg/mol or Z = 60).

Internal Modes

Following Monkenbusch et al.[19] the Thy-DAT bond lifetime is given by

$$\tau_b = 2 \times 10^{-4} \exp\left[\frac{5412}{T}\right] [\text{ns}] \tag{16}$$

If we consider an aggregate to be broken, when one bond opens, then $\tau_{agg} = \tau_b/(N_{agg} - 1)$ signifies the lifetime of an aggregate. This reduction of τ_{agg} compared to τ_b obviously underestimates the effective aggregate lifetime: if one bond breaks in a larger aggregate, much of the aggregate still exists. Furthermore, for small $N_{agg} \leq 2 \rightarrow \tau_b \leq \tau_{agg}$. Figure 8 presents the temperature dependence of both characteristic times.

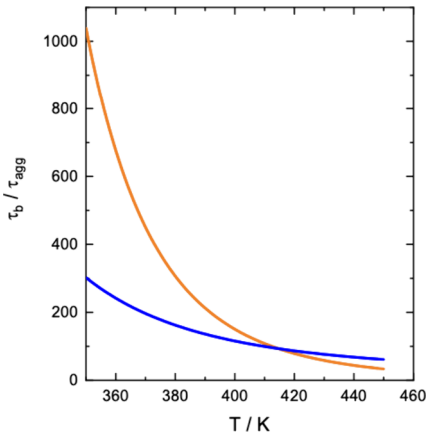

Figure 8. Temperature dependence of τ_{agg} (blue line) and τ_b (orange line) according to eq 16 and $\tau_{agg} = \tau_b/(N_{agg} - 1)$.

We observe that around T = 410 K τ_{agg} exceeds τ_b saying that for low N_{agg} the estimation for τ_{agg} is wrong.

From Sharma et al.[26] we know the temperature dependence of the Rouse rate Wl^4, allowing for a calculation of the entanglement time $\tau_e = \frac{d^4}{Wl4\pi^2}$ (tube diameter d_{PEO} = 49 Å)and the Rouse time $\tau_R = \frac{N^2 l_{seg}^4}{Wl4\pi^2}$. The bond lifetimes are taken from eq 16; the lifetimes of the aggregates are calculated as $\tau_{agg} = \tau_b/(N_{agg} - 1)$ with N_{agg} from the Table 4. Table 5 lists the results:

Table 5. Rouse Rates $Wl4$, Entanglement Time τ_e, Bond Lifetime τ_b, and Average Lifetime of an Aggregate τ_{agg}

T [K]	$Wl4$ [Å^4/ns]	τ_e [ns]	τ_R [ns]	τ_b [ns]	τ_{agg} [ns]
350	5810	100	601	1040	303
375	9700	60.2	360	370	179
415	19110	30.6	183	92.2	93
450	31480	18.6	111	33	61.7[a]

[a] For $\tau_{agg} > \tau_b$, τ_b is taken as aggregate lifetime

To contextualize the results, we compare the different characteristic times for our system. The relation between the Rouse times and the bond breaking and aggregate lifetimes suggests that only the internal modes of the building block contribute to the spectra. Since the terminal times for the weakly entangled PEO8K are longer than τ_R, this inequality also holds for 350 K. Thus, the corresponding aggregate

https://doi.org/10.1021/acs.macromol.5c03604
Macromolecules 2026, 59, 3508−3517

lifetimes are always shorter than the longest relaxation times of the building block. Following eq 1, modes bridging several blocks will be suppressed by the mode suppression factor $\exp\left[-\frac{\tau_p}{\tau_{agg}}\right]$ that accounts for the loss of the relaxation of longer bridging modes. From this we may conclude that the contributing internal mode spectrum of the aggregates will be close to identical to that of the PEO8K reference melt − a very minute change of the monomeric friction parameter due to the functionalized end may be safely neglected. The difference of the respective spectra has to be attributed to the changed diffusion contribution.

We note that the mode suppression phenomenon is a genuine finding of Monkenbusch et al.[19] and differs significantly from earlier work, where an acceleration of the internal aggregate relaxation by bond breaking was predicted.[3,18]

We demonstrate this prediction in describing the spectra from the melt of functionalized PEO8K chains by taking the internal mode spectrum of the reference melt. For the long-range center of mass diffusion we take the Fickian diffusion coefficients from PFG-NMR (Table 2). Figure 5 shows the result for the different temperatures. We observe that for all temperatures an excellent description of the spectra evolves.

Average Center of Mass Displacement of the Aggregates

The center of mass $\langle r_{com}{}^2(t)\rangle$ for the reference PEO8K melt at short times is characterized by subdiffusion with an exponent close to $\mu = \frac{1}{2}$. When $\langle r_{com}{}^2(t)\rangle \approx d^2$ reaches the size of the confining reptation tube d, a crossover to Fickian diffusion was observed. Its value agreed with that determined by PFG-NMR at much larger spatial (μm) and time scales (ms).

Then, how to model the center of mass motion of the aggregates? As demonstrated above, the lifetime of the aggregates is shorter than the terminal time of the PEO8K relaxations: The spectra reflect the internal dynamics of the single functionalized PEO8K component multiplied with the center of mass dynamic structure factor.

$$S(Q, t)_{com}/S(Q, 0)_{com} = \exp\left[-\frac{Q^2}{6}\langle r_{com}{}^2(t)\rangle\right] \tag{17}$$

For $\langle r_{com}{}^2(t)\rangle$ we model the cross over behavior, as described in eq 3. As Figure 5 shows, fixing the crossover parameters to those of the neat PEO8K melt ($\langle r_{com}{}^2(t_{cross})\rangle = 1780$ Å^2; $\mu \cong 1/2$) and employing the PFG-NMR Fickian diffusion coefficients (Table 2), we obtained a very good description of the data.

As at all investigated temperatures the aggregate lifetime is shorter than the longest relaxation time of the building block, aggregation cannot impose additional topological constraints on the center of mass motion of the aggregate. The effect of aggregation then results in an increased effective friction proportional to aggregation number N_{agg} of a specific associate. The ratio of the aggregate diffusion coefficient $D_{agg}(N_{agg})$ and the reference D_0 of the building block becomes

$$\frac{D_{agg}(N_{agg})}{D_0} = \frac{1}{N_{agg}} \tag{18}$$

The PFG-NMR experiments took place on time scales of ms, while all microscopic times are in the ns regime. Therefore, the NMR data were taken in the fast exchange limit, where different building blocks have changed very often their aggregate status. Then the average diffusion coefficient is just the thermal average over all aggregate diffusion coefficients $D_{agg}(N_{agg})$.

$$\bar{D}_{agg} = \sum_{N_{agg}=1}^{\infty} w(N_{agg})\, D_{agg}(N_{agg}) \tag{19}$$

With eqs 10 and 11 we have

$$\bar{D}_{agg} = \frac{\sum_{N_{agg}=1}^{\infty} D_0 N_{agg} p^{N_{agg}-1}(1-p)^2}{N_{agg}} = D_0(1-p)$$
$$= D_0 \frac{(1 + 4K_{agg}[H_0])^{1/2} - 1}{2K_{agg}[H_0]} \tag{20}$$

$\bar{D}_{agg}$ directly relates to the aggregation constant K_{agg} and the concentration of active chain ends H_0. In eq 20 all parameters are known from prior investigations. Figure 9 displays the predictions of eq 20 as a dashed line. The solid line displays the PFG-NMR result from Table 2 in an interpolated form $\left(D_{agg} = 511.2 \exp\left[-\frac{3354}{T}\right]\right)$ [Å^2/ns]. Obviously, eq 20 overpredicts the reduction of the diffusion coefficients in the aggregate melt.

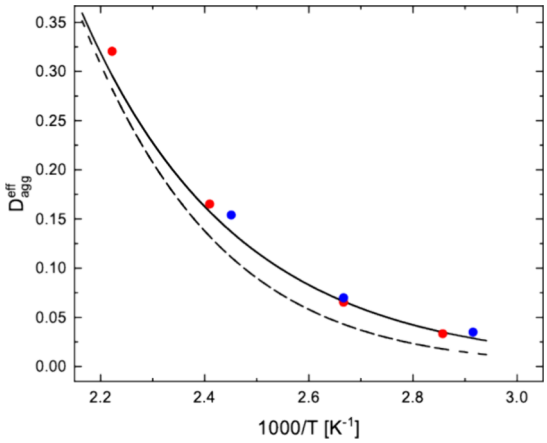

Figure 9. Average diffusion coefficients of the aggregates in their melt as a function of $1000/T$. The solid line displays the PFG-NMR result, the dashed line shows the prediction of eq 19, the red points represent the D^{eff}_{agg} based on eq 21 with $\alpha = 0.25$, and the blue points show the diffusion coefficients based on the SANS result.

From the evaluation of the SANS data, we found that a non-negligible fraction of the building blocks does not aggregate (weak DAT-DAT or Thy-Thy association or badly functionalized polymers). To consider this fraction, we need to modify eq 19 and allow for a nonaggregating fraction α. Then we have

$$D^{eff}_{agg} = D_0\alpha + (1-\alpha)\bar{D}_{agg} = D_{func} \tag{21}$$

With $D_0 \equiv D_{PEO8K}$ and D_{agg} from eq 19, we now evaluate D^{eff}_{agg} leaving α as an adjustable parameter. The comparison with the PFG-NMR results yields $\alpha \cong 0.25$, very close to the SANS result of $\alpha_{SANS} \cong 0.3$. The red points display the results from eq 21, the blue points show the corresponding diffusion coefficients based on the SANS results.

We observe very good agreement.

https://doi.org/10.1021/acs.macromol.5c03604
Macromolecules 2026, 59, 3508−3517

CONCLUSIONS

In our study of the association structure and dynamic of associating DAT-Thy functionalized melt of weakly entangled PEO chains we have achieved a nearly complete parameter-free understanding of the complex dynamics from the chain dynamics to Fickian diffusion. The chain dynamics was evaluated from a former investigation of the unfunctionalized reference melt. The association parameters were obtained from an earlier SANS study on a corresponding unentangled system of short PEO2K chains. The lifetimes of the H-bonds were taken from the NSE study of the PEO2K dynamics. Finally, in agreement with the sample characterization, the SANS data revealed a nonassociating fraction explaining the deviations of the aggregate diffusion coefficients from the prediction of polycondensation theory and justifying our assertion of a "parameter-free" description.

ASSOCIATED CONTENT

Supporting Information

The Supporting Information is available free of charge at https://pubs.acs.org/doi/10.1021/acs.macromol.5c03604.

Synthesis of the Thy and DAT functionalized PEOs, polymer characterization, NMR spectra, and SEC traces (PDF)

AUTHOR INFORMATION

Corresponding Author

Margarita Kruteva − *Jülich Center for Neutron Science, Forschungszentrum Jülich, 52428 Jülich, Germany;* orcid.org/0000-0002-7686-0934; Email: m.kruteva@fz-juelich.de

Authors

Jürgen Allgaier − *Jülich Center for Neutron Science, Forschungszentrum Jülich, 52428 Jülich, Germany;* orcid.org/0000-0002-9276-597X

Barbara Gold − *Jülich Center for Neutron Science, Forschungszentrum Jülich, 52428 Jülich, Germany*

Wim Pyckhout-Hintzen − *Jülich Center for Neutron Science, Forschungszentrum Jülich, 52428 Jülich, Germany;* orcid.org/0000-0002-1142-359X

Andreas Raba − *Jülich Center for Neutron Science, Forschungszentrum Jülich, 52428 Jülich, Germany*

Aurel Radulescu − *Forschungszentrum Jülich GmbH, Jülich Center for Neutron Science at MLZ, 85748 Garching, Germany*

Andreas Wischnewski − *Jülich Center for Neutron Science, Forschungszentrum Jülich, 52428 Jülich, Germany*

Michael Monkenbusch − *Jülich Center for Neutron Science, Forschungszentrum Jülich, 52428 Jülich, Germany;* orcid.org/0000-0001-6733-832X

Peter Falus − *Institut Laue-Langevin (ILL), 38042 Grenoble, France*

Dieter Richter − *Jülich Center for Neutron Science, Forschungszentrum Jülich, 52428 Jülich, Germany*

Complete contact information is available at: https://pubs.acs.org/10.1021/acs.macromol.5c03604

Notes

The authors declare no competing financial interest.

ACKNOWLEDGMENTS

We acknowledge Institute Laue Langevin (Proposal TEST-2660) and Heinz Maier-Leibnitz Zentrum at FRM-II for the neutron beamtime granted.

REFERENCES

(1) Xing, K.; Tress, M.; Cao, P. F.; Fan, F.; Cheng, S.; Saito, T.; Sokolov, A. P. The Role of Chain-End Association Lifetime in Segmental and Chain Dynamics of Telechelic Polymers. *Macromolecules* **2018**, *51* (21), 8561−8573.

(2) Alegría, A.; Arbe, A.; Colmenero, J.; Bhaumik, S.; Ntetsikas, K.; Hadjichristidis, N. Segmental and Chain Dynamics of Polyisoprene-Based Model Vitrimers. *Macromolecules* **2024**, *57* (12), 5639−5647.

(3) Granek, R.; Cates, M. E. Stress Relaxation in Living Polymers: Results from a Poisson Renewal Model. *J. Chem. Phys.* **1992**, *96* (6), 4758.

(4) Stukalin, E. B.; Freed, K. F. Minimal Model of Relaxation in an Associating Fluid: Viscoelastic and Dielectric Relaxations in Equilibrium Polymer Solutions. *J. Chem. Phys.* **2006**, *125* (18), 184905.

(5) Rubinstein, M.; Semenov, A. N. Thermoreversible Gelation in Solutions of Associating Polymers. 2. Linear Dynamics. *Macromolecules* **1998**, *31* (4), 1386−1397.

(6) Leibler, L.; Rubinstein, M.; Colby, R. H. Dynamics of Reversible Networks. *Macromolecules* **1991**, *24* (16), 4701−4707.

(7) Krutyeva, M.; Brás, A. R.; Antonius, W.; Hövelmann, C. H.; Poulos, A. S.; Allgaier, J.; Radulescu, A.; Lindner, P.; Pyckhout-Hintzen, W.; Wischnewski, A.; Richter, D. Association Behavior, Diffusion, and Viscosity of End-Functionalized Supramolecular Poly(Ethylene Glycol) in the Melt State. *Macromolecules* **2015**, *48*, 8933.

(8) Monkenbusch, M.; Krutyeva, M.; Pyckhout-Hintzen, W.; Antonius, W.; Hövelmann, C. H.; Allgaier, J.; Brás, A.; Farago, B.; Wischnewski, A.; Richter, D. Molecular View on Supramolecular Chain and Association Dynamics. *Phys. Rev. Lett.* **2016**, *117* (14), 147802.

(9) Lehn, J. M. *Supramolecular Chemistry: Concepts and Perspectives*; Wiley, 1995; pp 1−271,

(10) Brunsveld, L.; Folmer, B. J. B.; Meijer, E. W.; Sijbesma, R. P. Supramolecular Polymers. *Chem. Rev.* **2001**, *101* (12), 4071−4098.

(11) Stadler, F. J.; Pyckhout-Hintzen, W.; Schumers, J.-M.; Fustin, C.-A.; Gohy, J.-F.; Bailly, C. Linear Viscoelastic Rheology of Moderately Entangled Telechelic Polybutadiene Temporary Networks. *Macromolecules* **2009**, *42* (16), 6181−6192.

(12) Rossow, T.; Seiffert, S. Supramolecular Polymer Networks: Preparation, Properties, and Potential. *Adv. Polym. Sci.* **2015**, *268*, 1−46.

(13) Kang, J.; Miyajima, D.; Mori, T.; Inoue, Y.; Itoh, Y.; Aida, T. A Rational Strategy for the Realization of Chain-Growth Supramolecular Polymerization. *Science* **2015**, *347* (6222), 646−651.

(14) Kolomiets, E.; Buhler, E.; Candau, S. J.; Lehn, J.-M. Structure and Properties of Supramolecular Polymers Generated from Heterocomplementary Monomers Linked through Sextuple Hydrogen-Bonding Arrays. *Macromolecules* **2006**, *39* (3), 1173−1181.

(15) Brás, A. R.; Hövelmann, C. H.; Antonius, W.; Teixeira, J.; Radulescu, A.; Allgaier, J.; Pyckhout-Hintzen, W.; Wischnewski, A.; Richter, D. Molecular Approach to Supramolecular Polymer Assembly by Small Angle Neutron Scattering. *Macromolecules* **2013**, *46* (23), 9446−9454.

(16) Ahmadi, M.; Jangizehi, A.; Saalwächter, K.; Seiffert, S. Effect of Junction Aggregation on the Dynamics of Supramolecular Polymers and Networks. *Macromol. Chem. Phys.* **2023**, *224* (3), 2200389.

(17) Jankoski, P. E.; Masoud, A.-R.; Dennis, J.; Trinh, S.; DiMartino, L. R.; Shrestha, J.; Marrero, L.; Hobden, J.; Carter, J.; Schoen, J.; Phelan, H.; Smith, A. A.; Clemons, T. D. Bioactive Supramolecular Polymers for Skin Regeneration Following Burn Injury. *Biomacromolecules* **2025**, *26* (8), 5471−5482.

(18) Stukalin, E. B.; Freed, K. F. Minimal Model of Relaxation in an Associating Fluid: Viscoelastic and Dielectric Relaxations in Equilibrium Polymer Solutions. *J. Chem. Phys.* **2006**, *125* (18), 184905.
(19) Monkenbusch, M.; Krutyeva, M.; Pyckhout-Hintzen, W.; Antonius, W.; Hövelmann, C. H.; Allgaier, J.; Brás, A.; Farago, B.; Wischnewski, A.; Richter, D. Molecular View on Supramolecular Chain and Association Dynamics. *Phys. Rev. Lett.* **2016**, *117* (14), 147802.
(20) Sharma, A.; Kruteva, M.; Allgaier, J.; Hoffmann, I.; Falus, P.; Monkenbusch, M.; Richter, D. Chain Confinement and Anomalous Diffusion in the Cross over Regime between Rouse and Reptation. *ACS Macro Lett.* **2022**, *11* (12), 1343−1348.
(21) Brás, A.; Arizaga, A.; Agirre, U.; Dorau, M.; Houston, J.; Radulescu, A.; Kruteva, M.; Pyckhout-Hintzen, W.; Schmidt, A. M. Chain-End Effects on Supramolecular Poly(Ethylene Glycol) Polymers. *Polymers (Basel)* **2021**, *13* (14), 2235.
(22) Brás, A.; Arizaga, A.; Sokolova, D.; Agirre, U.; Viciosa, M. T.; Radulescu, A.; Prévost, S.; Kruteva, M.; Pyckhout-Hintzen, W.; Schmidt, A. Influence of Polymer Polarity and Association Strength on the Properties of Poly(Alkyl Ether)-Based Supramolecular Melts. *Macromolecules* **2022**, *55* (22), 10014−10030.
(23) Stejskal, E. O.; Tanner, J. E. Spin Diffusion Measurements: Spin Echoes in the Presence of a Time-Dependent Field Gradient. *J. Chem. Phys.* **1965**, *42* (1), 288−292.
(24) Fleischer, G.; Fujara, F. NMR as a Generalized Incoherent Scattering Experiment. In *Solid-State NMR I Methods*; Springer Berlin Heidelberg, 1994; pp 159−207. DOI: 10.1007/978-3-642-78483-5_4.
(25) Radulescu, A.; Pipich, V.; Frielinghaus, H.; Appavou, M. S. KWS-2, the High Intensity/Wide Q-Range Small-Angle Neutron Diffractometer for Soft-Matter and Biology at FRM II. *J. Phys. Conf Ser.* **2012**, *351* (1), 012026.
(26) Sharma, A.; Kruteva, M.; Allgaier, J.; Hoffmann, I.; Falus, P.; Monkenbusch, M.; Richter, D. Chain Confinement and Anomalous Diffusion in the Cross over Regime between Rouse and Reptation. *ACS Macro Lett.* **2022**, *11*, 1343−1348.
(27) Allgaier, J.; Hövelmann, C. H.; Wei, Z.; Staropoli, M.; Pyckhout-Hintzen, W.; Lühmann, N.; Willbold, S. Synthesis and Rheological Behavior of Poly(1,2-Butylene Oxide) Based Supramolecular Architectures. *RSC Adv.* **2016**, *6* (8), 6093−6106.
(28) Krajenta, J.; Polinska, M.; Lapienis, G.; Pawlak, A. The Crystallization of Poly(Ethylene Oxide) with Limited Density of Macromolecular Entanglements. *Polymer* **2020**, *197*, 122500.
(29) Read, D. J. Mean Field Theory for Phase Separation during Polycondensation Reactions and Calculation of Structure Factors for Copolymers of Arbitrary Architecture. *Macromolecules* **1998**, *31* (3), 899.
(30) Carothers, W. H. Polymers and Polyfunctionality. *Trans. Faraday Soc.* **1936**, *32* (0), 39−49.

https://doi.org/10.1021/acs.macromol.5c03604
Macromolecules 2026, 59, 3508−3517